PRAMANA
— journal of
physics

Supplement to Vol. 41
December 1993
pp. 197–216

Recent results from the DØ detector

RAJENDRAN RAJA
Fermi National Accelerator laboratory, Batavia, Illinois 60510, USA
(for the D0 Collaboration)

Abstract. The DØ Experiment started taking data in August 1992. We present preliminary results on inclusive jet production, direct photon production, W/Z production and decays, b Physics and first searches for $t\bar{t}$ production and new particles beyond the Standard Model.

1. The DØ detector

The DØ detector [1,2] was commissioned early this year after a period of 8 years in the making and began taking data in August 1992. It was possible to shorten the engineering period in DØ and move directly into a Physics data mode largely in part due to the automated Alarms and Monitoring Control system. The detector consist of three main parts, the central tracker, the Uranium Liquid argon Calorimeter and the muon System. There is no central magnetic field in DØ leading to a compact hermetic calorimeter and a consequent reduction in the amount of decay background from π and K decays. The detector is shown in figure 1.

1.1. Central tracking system

The Central Tracking System [1], shown in figure 2, consists of four main components: Vertex Chamber, Transition Radiation Detector, Central Drift Chamber and two sets of Forward Drift Chambers. The Vertex Chamber [1] has three cylindrical layers of jet-type cells, and every cell in a layer has eight sense wires. It has an intrinsic resolution in azimuth of $60\mu m$. It is capable of separating two tracks that are separated by more than 0.6 mm. The chamber can also used to find secondary vertices, and provide rejection against conversions in the Transition Radiation Detector by demanding a track in the vertex chamber.

The Transition Radiation Detector [1] provides additional rejection of pions in the identification of central electrons. It has three cylindrical layers, each layer consisting of a set of polypropylene foils surrounded by a radial drift X-ray detector. A pion rejection factor of 50 has been achieved in test beam conditions for an electron efficiency of 90%. It should be emphasized that test beam conditions where single isolated electrons are compared to single isolated pions do not simulate the data taking environment of high multiplicity events.

The Central Drift Chamber [1] has four cylindrical layers of jet-type cells, and every cell in a layer has seven sense wires. It provides a spatial resolution of

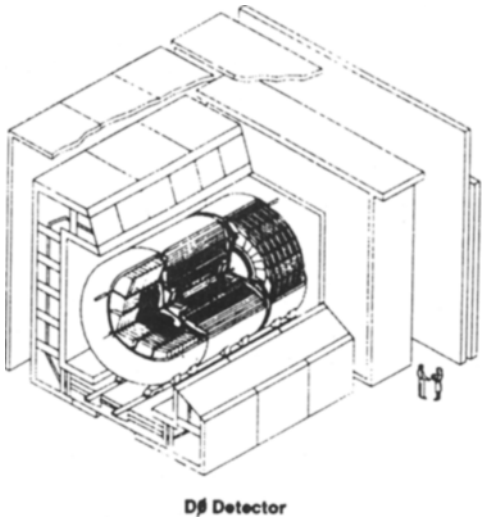

Figure 1. The DØ Detector

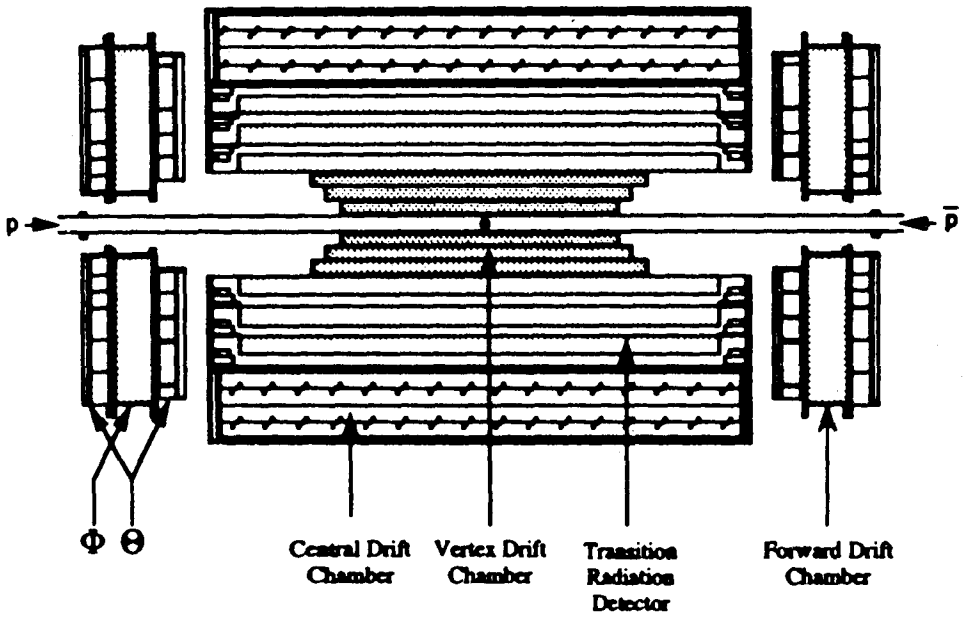

Figure 2. The DØ Central Tracking System.

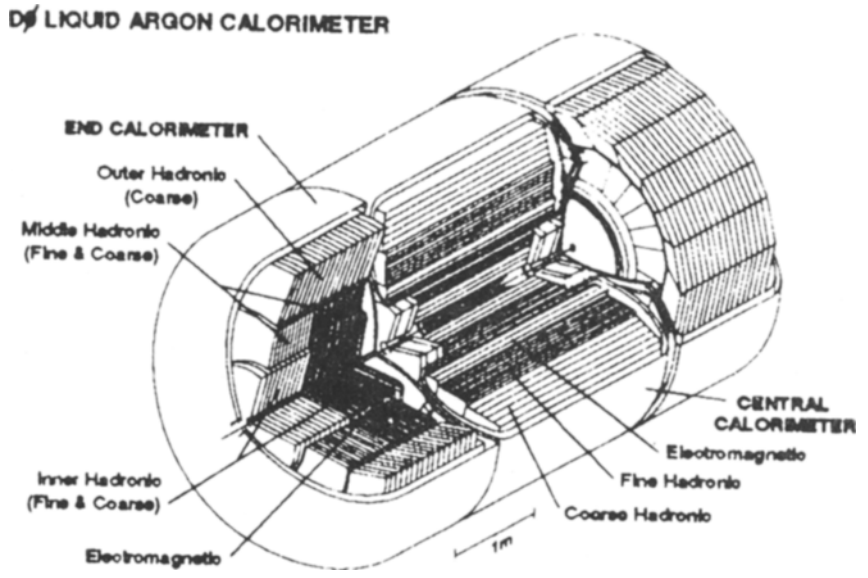

Figure 3. The DØ Calorimeter System.

150 μm in the azimuthal direction and a resolution along the beam direction of 4 *mm* with the help of delay lines. By measuring the pulse heights of track signals, the Central Drift chamber provides good separation between minimum ionizing and twice minimum ionizing tracks.

The Forward Drift Chambers [1] cover angles down to 5°, and include Φ and Θ measuring units. The Φ measuring units have radial sense wires, with 16 measurements per track. The Θ units have sense wires that are transverse to the beam, with 8 measurements along each track in each of the two units. The spatial resolution is 200 μm for all units.

1.2. Calorimeter system

The DØ calorimeter is a sampling calorimeter made of uranium as the absorbing material and liquid argon as the sampling medium. Uranium, being of high density, leads to a compact calorimeter design . It also provides a mechanism for getting nearly equal electromagnetic to hadronic response by suppressing the response to EM showers. This leads to good resolution and linearity in the hadronic response.

The DØ Calorimeter System [1], shown in figure 3, consists of a Central Calorimeter with 32 modules arranged azimuthally parallel to the beam. The two End Calorimeters cover angles down to pseudo-rapidities of 4.5 . Each of the three calorimeters contains an electromagnetic section with thin uranium plates, a fine hadronic section with thick uranium plates, and a coarse hadronic section with thick copper or steel plates. Printed circuit boards with segmented detection pads are interleaved between the absorber plates to detect the ionization in the liquid argon. During the design stage, extensive Monte Carlo simulations with full showering was used to insure that the Calorimetry was as hermetic as possible.

Liquid argon permits fine segmentation of the calorimetry. Each electromagnetic section is divided into 4 segments longitudinally (for a total of 21 X_o), and

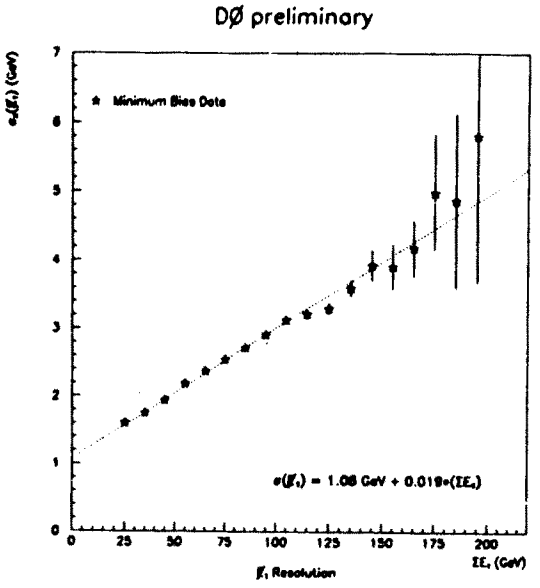

Figure 4. The standard deviation of the x component of the $\not\!\!E_T$ as a function of scalar transverse energy. The line is a linear fit to the data.

the hadronic sections are divided into 4–5 depths (for a total of 7–9 λ). The transverse segmentation is 0.1 × 0.1 for $\Delta\eta \times \Delta\phi$, except in the third electromagnetic longitudinal section (where shower maximum occurs), where the segmentation is doubled for better position resolution of the EM shower.

The fractional energy resolution of electrons in the calorimeters is $(\sigma/E)^2 = (0.003)^2 + (0.157)^2/E + (0.29)^2/E^2)$ and of pions is $(\sigma/E)^2 = (0.05)^2 + (0.50)^2/E + (0.30)^2/E^2)$. The spatial position resolution for electrons is 1–2 mm, for energies above 50 GeV. The e/π response of the calorimeter system is energy dependent but has been measured in a test beam to be in the range 1.04–1.12 for energies between 10 and 100 GeV.

The missing transverse energy $\not\!\!E_T$ resolution of the DØ Calorimeter System, important for new particle searches and the precision measurement of the mass of the W boson, is excellent because of the calorimeter's hermeticity. The Inter Cryostat detector of scintillators placed between the central and end cap calorimeters enhances the $\not\!\!E_T$ resolution . The standard deviation of the x component of the $\not\!\!E_T$ is plotted as a function of total scalar E_T in figure 4. The $\not\!\!E_T$ resolution is 2–4 GeV for scalar E_T in the range 50–150 GeV.

1.3. Muon system

The Muon System [1] is made up of five iron toroids, 1.1–1.5 meters thick, and three layers of proportional drift tube (PDT) chambers. The central toroid covers angles down to 45°. The end toroids and the small angle muon system cover the forward region down to 5°. Thus there is full muon coverage for $|\eta| \leq 3.2$. The momentum of a muon is determined by using the PDT chambers to measure the

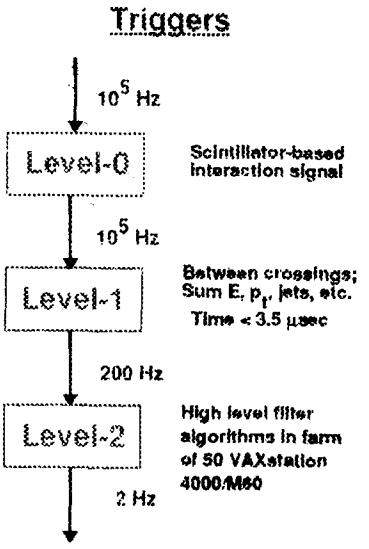

Figure 5. The DØ Trigger System.

deflection of the muon trajectory in the 1.9 Tesla steel toroids. The momentum resolution, $\delta p/p = 0.2 + 0.01p$, is dominated by multiple scattering for momenta < 80 GeV/c. The combined calorimeter plus toroid thickness varies from 14 λ in the central region to 19 λ in the end regions. This thickness reduces backgrounds from hadronic punchthroughs to a negligible level.

1.4. Trigger

The DØ Trigger System [1] is shown in figure 5. The initial (Level 0) trigger uses scintillation counters on both sides of the interaction point that fire when an inelastic collision takes place. This minimum bias trigger rate depends on the luminosity, but is typically 100 kHz. The next (Level 1) trigger is a hardware trigger that determines whether the event has jets, high $\not\!\!E_T$, High E_T EM clusters and muons. The Level 1.5 trigger uses more information from the muon chambers to determine the p_T of the muons. The Level 1/1.5 rate at the present time is 70 Hz, which will be increased to 200 Hz in the near future.

The Level 2 trigger [1] is a software filter running on a farm of VAX 4000/60 microprocessors. Using algorithms similar in style to those used in the offline code, electrons, $\not\!\!E_T$ scalar E_T and muon triggers are developed and the event rate from Level 1 is cut to $1.5 \sim 2$ HZ . This rate out of level 2 is expected to rise in the near future to 4 Hz. Events are then written to Exabyte high density tape and the offline processing is done on a Unix Farm of 20 MIP processors. Results in the form of data summary tapes are put on a file Server array of disks and are served out to individual users working on their workstations.

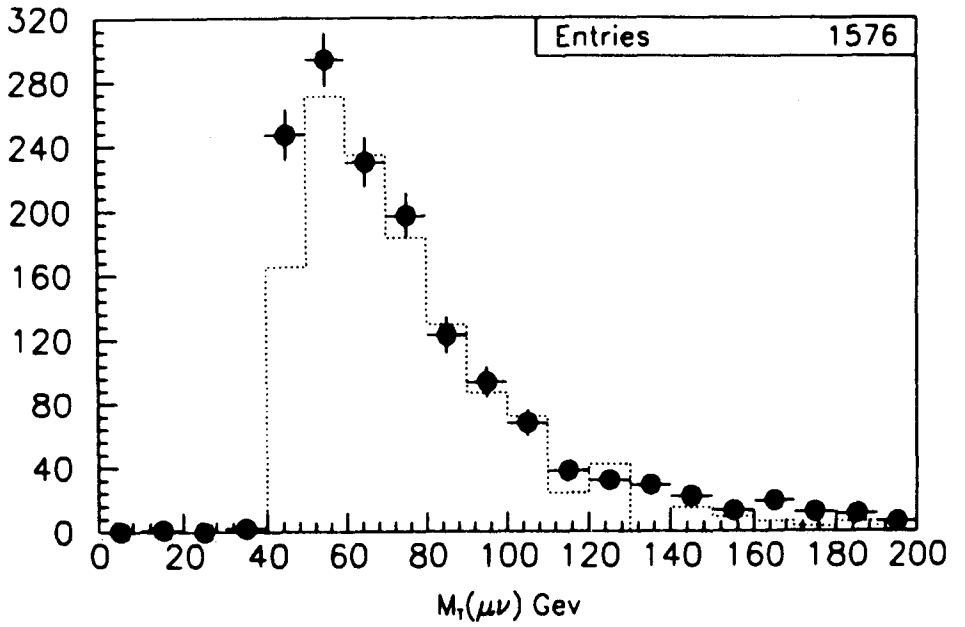

Figure 6. W transverse mass for $W \rightarrow \mu\nu$ events. The dashed line is the Monte Carlo estimate for the signal which does not include backgrounds

2. Preliminary Physics Results

2.1. Electroweak physics

We present results based on 7.5 pb^{-1} of data on the channels $W \rightarrow \mu\nu$ and $Z \rightarrow \mu\mu$ [3]. Only central muons within pseudo-rapidity $|\eta| < 1.7$ were selected for this analysis. For the W sample, events with $p_T(\mu) > 20\,GeV/c$ and calorimeter $E_T > 20\,GeV$ were selected offline. Cosmic ray background events were eliminated using track quality cuts. Backgrounds from QCD induced muons were brought under control by demanding calorimeter isolation. Figure 6 is the transverse mass of the resulting Ws. The dashed line is the prediction of the Monte Carlo. The Monte Carlo does not include contributions from instrumental backgrounds such as cosmics that may be left over after cuts. The long tail in the transverse mass in the muon sample is due to the resolution of the muons. Figure 7 is the p_T spectrum of the Ws decaying into muons. Superimposed is the corresponding quantity due to Ws decaying to electrons. Since the p_T measurement of the W does not involve the final decay products (the neutrino E_T is an inferred quantity), the two curves show excellent agreement. The value of $\sigma.B(W \rightarrow \mu\nu)$ thus measured is 2.00 $\pm 0.07(stat)$ $\pm 0.41(sys)$ $\pm 0.24(luminosity)$ nb. The value of $\sigma.B(Z \rightarrow \mu\mu)$ thus measured is 0.20 $\pm 0.02(stat)$ $\pm 0.05(sys)$ $\pm 0.02(luminosity)$ nb.

In order to measure the W/Z mass difference, we need to use the decay modes into electrons. This is due to the superior ability of DØ to measure electrons. We report in this channel on 8.8 pb^{-1} of data. For the channel $Z \rightarrow ee$, electrons

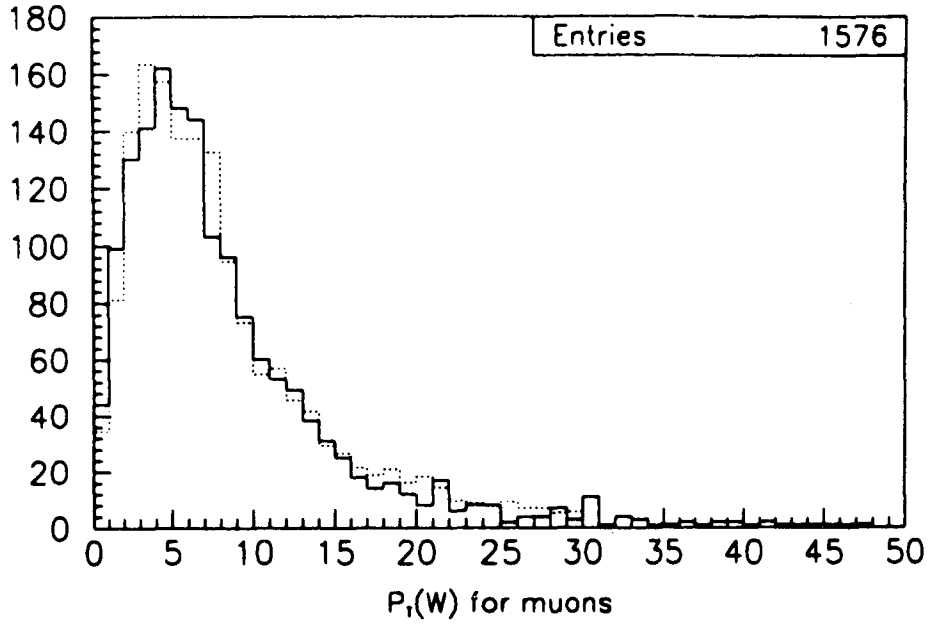

Figure 7. p_T spectrum of W decays to muons. The dashed line is the corresponding quantity for W's decaying to electrons.

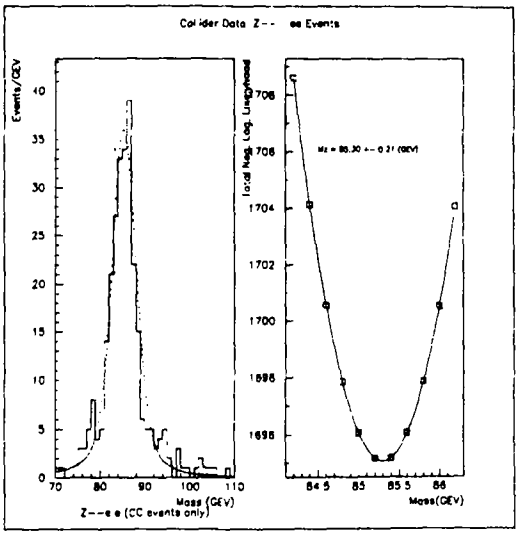

Figure 8. Di-electron invariant mass distribution clearly showing a Z peak

were selected offline with $p_T > 20\ GeV$, [4] and shape cuts were applied on the energy deposition in the calorimeter. Tracks in the central tracker that point to the electromagnetic cluster centroid within errors were required, for the electron to be identified as such. Figure 8 shows the effective mass of the di-electron pair, showing a clear Z peak, where both electrons were detected in the central calorimeter. The fitted curve is the result of an unbinned maximum likelihood fit.

Figure 9 is the transverse mass of the sample of W's decaying into electrons obtained by demanding an electron with $E_T > 20\,GeV$ and $\not\!\!E_T > 20\,GeV$. A clear W Jacobian peak is seen. Superimposed is the result [5] of a fit to the W transverse mass that is based on a higher order QCD model of the W p_T spectrum. The electron calibration in DØ is still being understood ,as can be seen by the position of the Z peak, so we are not in a position to quote final numbers for the W/Z mass difference. Based on 3.4 pb^{-1} of data, we have also measured the quantities $\sigma.B(W \rightarrow e\nu)$ to be $2.48 \pm 0.05(stat) \pm 0.26(sys) \pm 0.30(luminosity)$nb and $\sigma.B(Z \rightarrow ee)$ to be $0.235 \pm 0.19(stat) \pm 0.40(sys) \pm 0.028(luminosity)$nb. This is consistent with the values measured in the μ channel and also with other measurements.

2.2. Top

2.2.1. Introduction

The Standard Model [6,7] requires the existence of the top quark to complete the three generations of quarks and leptons. Lower bounds up to 91 GeV/c^2 have been reported [8-11] for the top quark mass and precision measurements of electroweak parameters predict the mass of the top quark to be $152 \pm 17 \pm 21\ GeV/c^2$ [12], which assumes the completeness of the Standard Model. The dominant mode of top quark production at the Tevatron is via parton fusion into $t\bar{t}$ [13-15]. Since the top quark is now established to be heavier than the W boson, each top quark will decay into a real W. Each W then decays leptonically into a charged lepton and neutrino or hadronically into a pair of quarks. The branching ratio for both

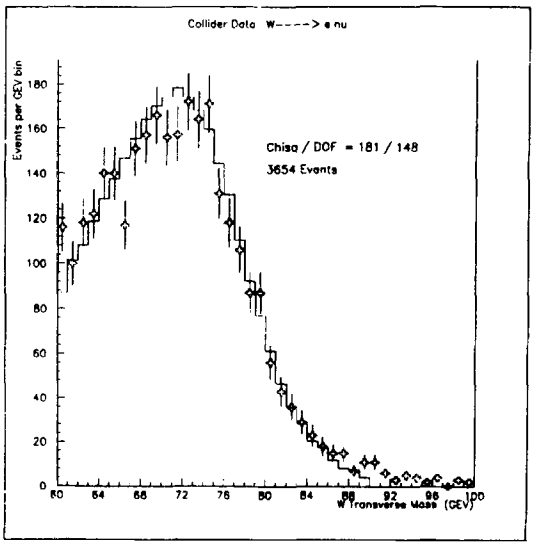

Figure 9. W transverse mass for $W \rightarrow e\nu$ events. The points are the data. The histogram is the result of the fit discussed in the text.

W's from a $t\bar{t}$ pair to decay into an $e\mu$ pair is $\frac{4}{81}$ and into an ee pair is $\frac{1}{81}$. The channels where both the W's decay leptonicaly is relatively background free and we choose to study these channels in this paper. The signature for a top quark event then is two high p_T leptons accompanied by at least two jets (from the decay of the associated b quark) and significant missing transverse momentum due to the emission of undetected neutrinos from the W decay.

2.2.2. ee event selection

The total integrated luminosity being reported here for the ee channel is $7.3 \pm 0.88\, pb^{-1}$. For electrons used in this analysis, we demand the logical OR of three level 1 trigger and level 2 conditions. 1) One level 1 electromagnetic(EM) tower with $E_T > 14$ GeV which produces an isolated level 2 electron candidate with $E_T > 20$ GeV and level 2 missing $E_T > 20$ GeV. 2) Two level 1 EM towers with $E_T > 7$ GeV and two isolated electron candidates with $E_T > 20$ GeV at level 2. 3) One level 1 EM tower with $E_T > 20$ GeV , two level 1 jet towers with $E_T > 5$ GeV leading to one level 2 electron candidate with $E_T > 15$ GeV , two level 2 jets with $E_T > 16$ GeV and level 2 missing $E_T > 20$ GeV. In this trigger , an electron may simultaneously satisfy level 1 electron and jet conditions.

The offline event selection cuts were chosen to retain good efficiency for top decays while minimizing backgrounds. We impose covariance matrix conditions on the shape of the calorimeter electron energy deposition ($\chi^2 < 200$) which were determined from test beam data [4]. We also demand a good central detector track matched with the calorimeter centroid of the electron for one of the electrons. The offline cuts for the ee analysis thus demand two electrons with $E_T > 15$ GeV, missing $E_T > 20$ Gev and 2 jets with $E_T > 20$ GeV. We also eliminate Z decays to electrons by removing electron pairs with effective mass $\pm 14\, GeV/c^2$ about the

Z peak. Events with jets which deposit more than 40% of their energy in the Inter Cryostat detector are also removed from the sample. The efficiency of the calorimeter electron identification cuts has been determined to be 90% from W decays. The efficiency for track finding has been estimated to be 80% from $Z \rightarrow ee$ decays. Taking into account the correlation between the efficiencies of the trigger and offline cuts, we determine overall efficiencies for our ee event selection as a function of the top mass. Note that the efficiency for triggering and selection of ee candidates from $t\bar{t}$ decays goes up with top mass because the average energy of the electrons increases. The ee event selection efficiencies have an error of 15% on them which include systematic and statistical uncertainties.

2.2.3. $e\mu$ event selection

In this channel we have used an integrated luminosity of $7.5 \pm 0.9\ pb^{-1}$ using the three different trigger configurations: EM cluster + muon, EM cluster + $\geq$ 2jets and muon + $\geq$ 2jets. The following level 2 trigger requirements were imposed for the three configurations. One EM cluster $E_T > 7\ GeV$ and a muon with $p_T > 5\ GeV, |\eta| < 1.7$ for the EM cluster + muon channel; one EM cluster $E_T > 12\ GeV$ and two or more jets with $E_T > 16\ GeV$ and missing $E_T > 20\ GeV$ in the EM cluster +$\geq$ 2 jets channel; and a muon with $p_T > 5\ GeV, |\eta| < 1.7$, one jet with $E_T > 25\ GeV$, another jet with $E_T > 15\ GeV$ and missing $E_T > 12\ GeV$ in the muon + $\geq$ 2jets channel. Further offline requirements were imposed on the EM cluster, (covariance matrix $\chi^2 < 200$, $E_T > 15\ GeV$ with $|\eta|$ <2.5) and the muon ($p_T > 15$ GeV and $|\eta|$ <1.7). Next we suppress backgrounds from non-top conventional processes by requiring that both leptons be isolated in the calorimeter and that the minimum $\eta - \phi$ separation, $\Delta R(\equiv \sqrt{\delta\phi^2 + \delta\eta^2})$ be at least 0.25 between the electron and the muon. These cuts remove a substantial fraction of the backgrounds from QCD multijet events and from radiative $W \rightarrow \mu\nu$ and $Z \rightarrow \mu^+\mu^-$ events. We then require that the missing $E_T > 20$ GeV and at least two reconstructed hadronic jets of $E_T > 12$ GeV and 10 GeV . These cuts remove most of the backgrounds for $Z \rightarrow \tau^+\tau^-$ decays, $Z \rightarrow b\bar{b}$ decays and W^+W^- and WZ pair production. Since the electron has no track match requirements in this channel, we do pick up wide angle bremsstrahlung events from $W \rightarrow \mu\nu$. We reject these with cuts on the transverse mass $M_T(\mu\gamma\nu)$ consistent with wide angle bremmstrahlung events. The $e\mu$ event selection efficiencies have an error of 23% on them which includes systematic and statistical uncertainties.

To arrive at these numbers we have used the ISAJET event generator program [16] and the GEANT based DØ detector simulation program [17].

2.2.4. Results

Figure 10 shows the scatter plot of the missing E_T of the electrons in the effective mass of the electron pair for the ee sample. Figure 11 shows the corresponding distributions for top quark decays of mass 140 GeV/c^2 ($\int Ldt = 2.7 fb^{-1}$). It can be seen that if top quark decays are present, a substantial fraction of these should populate the region with missing E_T's greater than 20 GeV . The concentration of events in the data for ee effective masses between 70 GeV/c^2 and 100 GeV/c^2 is due to the Z boson. After the cuts described in section 2.2.2, we have no candidates events left.

Figure 12 shows a scatter plot of the p_T of the muon vs E_T of the electron in the $e\mu$ sample for data. Figure 13 shows the corresponding plot for 120 GeV/c^2

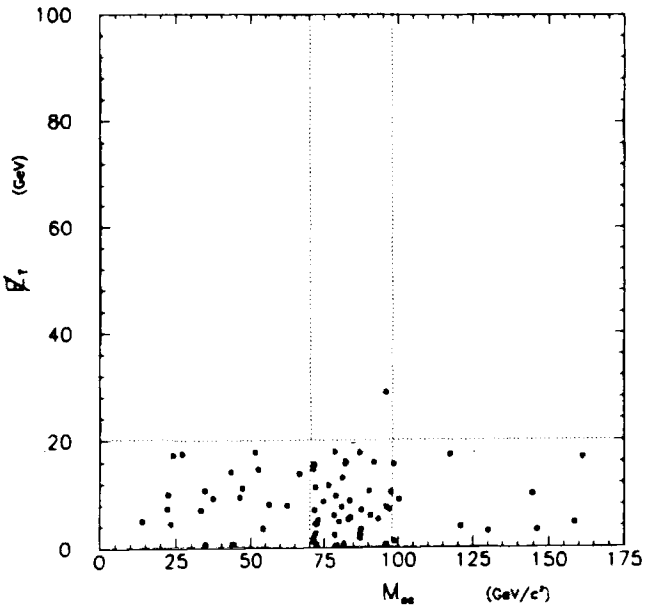

Figure 10. Missing E_T vs. mass of the ee pair for DØdata.

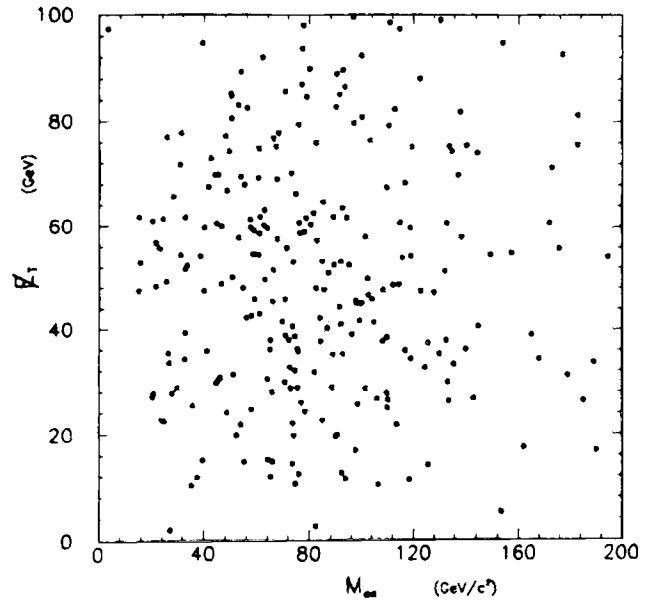

Figure 11. Missing E_T vs. mass of the ee pair for $t\bar{t} \rightarrow ee$ Monte Carlo for $m_t = 140\, GeV/c^2$

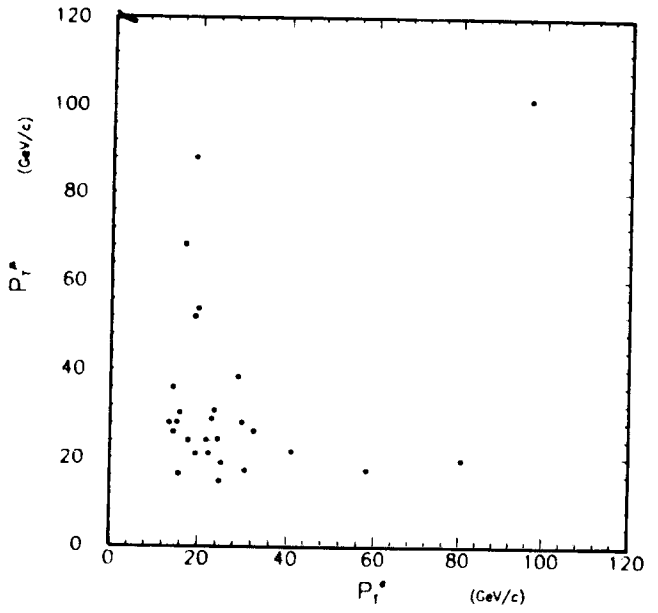

Figure 12. p_T of muon vs E_T(e) for DØ data

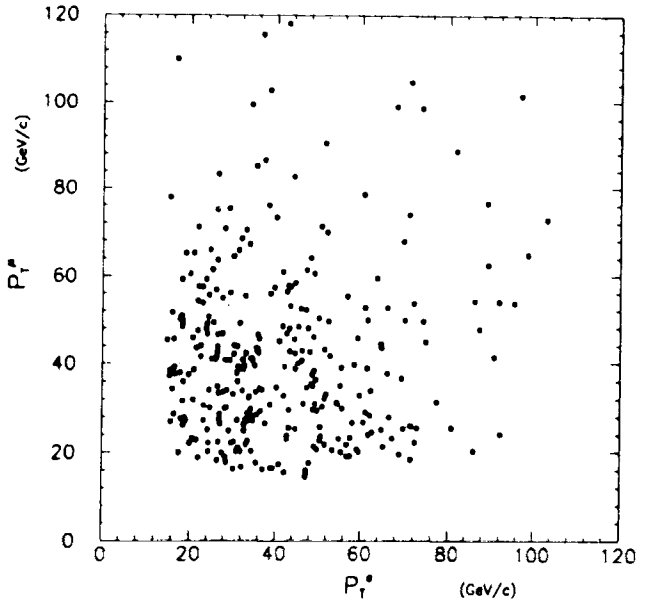

Figure 13. p_T of muon vs E_T(e) for $t\bar{t} \rightarrow e\mu$ Monte Carlo for $m_t = 120\, GeV/c^2$

top decays ($\int Ldt = 1.2 fb^{-1}$). It can be seen that a substantial portion of the top decays will survive the cuts on the muon and electron transverse momenta. After all the cuts described in section 2.2.3 are imposed on the data, one event remains of which more will be said later.

2.2.5. Estimation of backgrounds and the top limit

In order to estimate the backgrounds that survive the above cuts, we have generated $Z \rightarrow \tau\tau, Z \rightarrow b\bar{b}$, $W + Jets$, WW, WZ and radiative $W(Z) \rightarrow \mu + X$. Additionally we have tried to estimate instrumental backgrounds due to misidentification of electrons, mismeasurements leading to fake missing E_T, muons from π/K decays in flights and cosmic ray muons. Instrumental backgrounds were estimated using data as well as Monte Carlo events. For an integrated luminosity of $7.3\, pb^{-1}$, we estimate a total of 0.23 background events above the cuts from all the sources listed in the ee channel. For an integrated luminosity of $7.5\, pb^{-1}$, we estimate a total of 0.65 background events above the cuts from all the sources listed in the $e\mu$ channel.

Figure 14 shows the 95% upper limit estimate of the $t\bar{t}$ cross section using the ee and $e\mu$ analyses combined, including the one event observed. The two curves shown are for the two cases where background is subtracted and no background is subtracted from the total expected number of events. We note that zero background subtraction leads to a more conservative limit. Using the cross sections quoted in Berends et al [15] we set a lower limit at 95% confidence limit of 103 GeV/c^2 for the background subtracted case and $99\, GeV/c^2$ for the zero background subtracted case for the top mass.

2.2.6. The remaining $e\mu$ event

The single event (Run 58796 event 417) in the $e\mu$ plot that is well above the cuts merits further discussion. While we make no claim that we have observed production of the top quark or indeed any other new phenomenon, it is interesting to hypothesize that this event is due to $t\bar{t}$ production and decay to $e\mu$. The electron quality is excellent ($\chi^2 = 51$)and further confirmation is obtained from the information in the Transition Radiation Detector (TRD). The muon momentum in the event is measured reasonably well $p_T(\mu) = 110^{+\infty}_{-50}\, GeV/c$. The muon is missing hits in the first layer of the muon chambers, indicating that it probably transited between two chambers in that layer. The muon track is found in the two muon chamber layers after the toroid and is confirmed by minimum ionizing energy deposition in the calorimeter and a central detector track when extrapolated to the vertex. The error on the muon momentum is approximately Gaussian in $1/p$ and $p_T(\mu)$ is 5σ above the 15 GeV/c event selection cut imposed on it. The missing E_T value is $74^{+\infty}_{-7}\, GeV$. It is somewhat correlated with the muon momentum. It value cannot be smaller than 67 GeV for any muon momentum. It can be seen that the missing E_T vector is at almost right angles to the muon and is not influenced greatly by the muon resolution. Both the muon and the electron are well isolated. The event has three jets with $E_T'^s$ of (30 ± 5) GeV, $(28 \pm 5\, GeV)$ and $(14 \pm 2)\, GeV$. The backgrounds considered above are unlikely to produce this event.

Under the hypothesis that the highest E_T jets from this event are due to the $b\bar{b}$ produced in $t\bar{t}$ decays , we have attempted to extract information on the mass of the top quark using extensions of techniques similar to those proposed by Dalitz et al [18]. We find that the top mass cannot be lower than 130 GeV/c^2 at 95 % C.L.

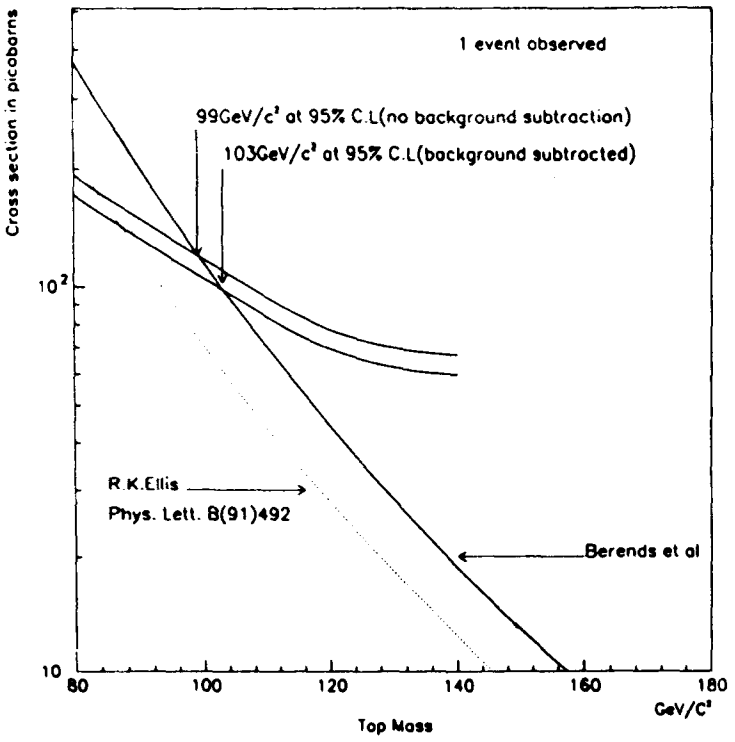

Figure 14. Cross section for $t\bar{t}$ production as a function of top mass . First curve shows our 95% upper limit deduced from ee and $e\mu$ analysis combined with zero background assumed. The second curve shows our background subtracted result.

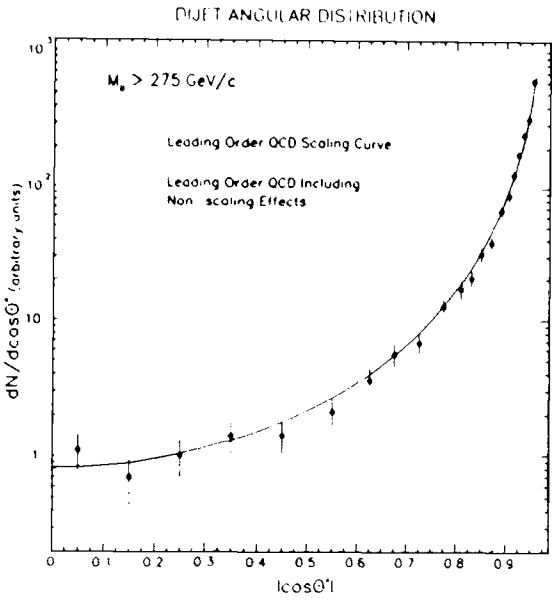

Figure 15. Angular distribution of di-jet events in the jet-jet center of mass for jet pairs with effective mass greater the 275 GeV/c^2

The upper limit is still being studied rigorously but is unlikely to be much higher than 170 GeV/c^2.

2.3. QCD

DØ being a hermetic calorimeter is ideally suited for the study of QCD phenomena. We define jets as clumps of energy falling in a cone in $\Delta\eta \times \Delta\phi$ space of radius 0.7. We present here data from 4 pb^{-1} of [19,20] data and E_T of the jet greater than 30 GeV. Figure 15 shows the distribution of the cosine of the center of mass angle in the di-jet rest frame, for jet pairs having effective mass greater than 275 GeV/c^2. The dashed curve is the leading order QCD scaling curve with no running in the coupling constant. The full curve, which fits data much better has the QCD scale breaking effects. Inclusive jet cross sections have been measured. Comparison with theory shows agreement, but is currently awaiting better calibration of the energy scale of the detector in order to reduce systematic errors.

Figure 16 shows the distribution of the variable χ defined as $(1 + cos\theta^*)(1 - cos\theta^*)^{-1}$. For Rutherford scattering , it is easy to show that the distribution in χ is flat. The data once again favor QCD with scaling violation. It should be pointed out that this DØ measurement extends the previous measuring range of χ by almost a factor of two, a result largely due to our excellent coverage in the forward direction. Figure 17 shows the E_T spectrum of direct photons produced in the DØ experiment. Photons were defined in much the same way as electrons, but without the requirement of the central detector track. The problem here lies in distinguishing photons that are directly produced by quark bremsstrahlung from

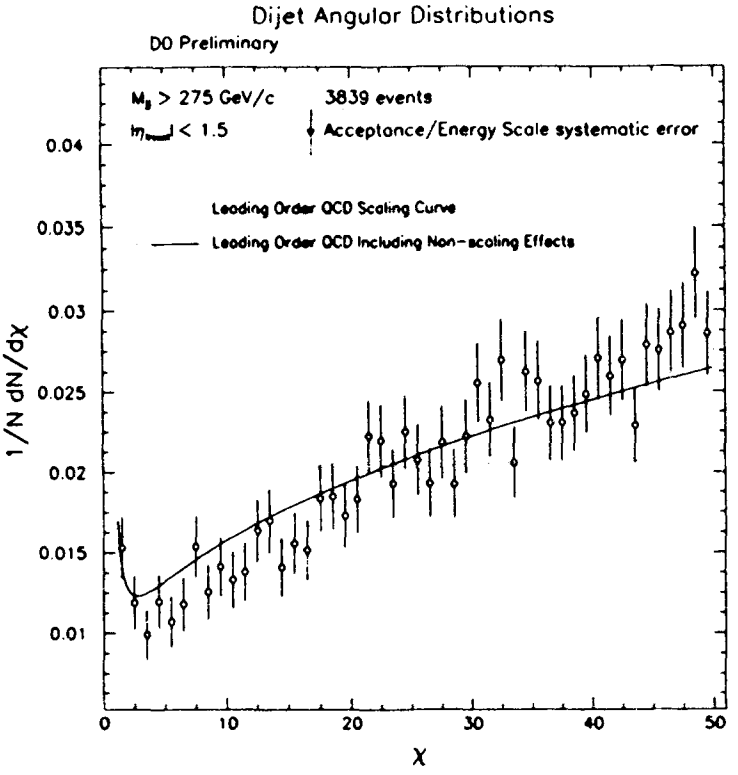

Figure 16. Distribution of the χ variable for dijet effective masses greater than 275 GeV/c^2. Again, effects due to scale breaking can be seen clearly

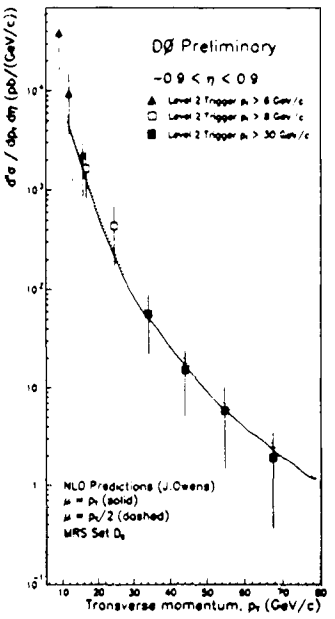

Figure 17. E_T spectrum of direct photons in DØ

those produced by the decay of π^0 mesons. Two methods are used to estimate the signal/background ratio as a function of E_T. One relies on looking for photon conversions in the tracker. Since π^0's produce two photons, they are twice as likely to convert as single photons. Also, DØ has a detailed simulation of the detector, which can be used estimate the π^0 contamination. Both methods yield a ratio $\gamma/\pi^0 \sim 0.42$. It can be seen that the measured DØ direct photon spectrum is in moderately good agreement with the next to leading order QCD predictions.

2.4. b Physics

As of this writing, DØ has observed same sign dimuon production attibutable to $B\bar{B}$ mixing, opposite sign dimuon production which shows J/ψ and Υ peaks. Using the inclusive single muon channel, one can also measure associated $b\bar{b}$ and $c\bar{c}$ production. For $B\bar{B}$ mixing studies, we have analyzed 3.5 pb^{-1} of data. We require both muons to be within $|\eta| < 1.0$. We require the muons to pass through field regions in the toroid such that $\int B.dl > 0.67$ Tesla meters so that momentum measurement is done well and the charge of the muon can be unambiguously inferred. We require the muons to be non-isolated such as would be expected from b jet fragmentation. Cuts are also made to clean the sample of cosmic ray background. We measure a value of the mixing parameter [21]

$$\chi = \frac{Probability(b \to \bar{B}^0 \to B^0 \to \mu^+)}{Probability(b \to \mu^\pm)} = 0.21 \pm 0.05(stat) \pm (0.04)(sys).$$

We observed J/ψ produciton in both isolated and non-isolated di-muons, suggesting that J/ψ 's are produced from the decay of B mesons in b quark jets as well as directly via gluon fusion. We quote a J/ψ production cross section $\times$ branching

ratio [22] of $0.92 \pm 0.10(stat) \pm 0.46(sys)$ nb for p_T of the $J/\psi > 8GeV/c$ and $|\eta| < 0.8$.

We have also tried to account for the rate of single muon production in jets by a model incorporating charm and bottom quark decays, as well as the rarer light (strange, up and down) quark decays to muons. The model works well, in as much as that the observed single muon p_T spectrum is well accounted for by the predictions of the Monte Carlo cocktail [23].

2.5. New Particle Searches

In the area of new particle searches , DØ is looking for Supersymmetry (gluinos and squarks), that leave a tell-tale signature of cascade deacys into leptons and jets accompanied by significant $\not\!\!E_T$. At present, we have no results to report in this channel as yet. Work is in progress. In the area of lepto-quarks, DØ has carried out a search [24] for composite objects that carry both baryon and lepton number. These objects are predicted within certain supersymmetric and composite models. The leptoquarks are produced in pairs . Each leptoquark can decay into either charged or neutral lepton + quark jet. So the signature for leptoquark pair production is either 2 charged leptons + 2 jets or one charged lepton, $\not\!\!E_T$ + 2 jets. We have searched for the case where the charged lepton is an electron. In 7.5 pb^{-1} of data, we see no events which satisfy the criteria imposed by the topology of the final state. Assuming a 100% branching ratio into electrons, we can set a 95% CL lower bound of 126 GeV/c^2 for the leptoquark mass. If we assume a 50% branching ratio into electrons, the bound is at 109 GeV/c^2 .

3. Conclusion

To conclude, the DØ detector has had a remarkably rapid turn on. Run 1a at Fermilab is over with 16.7 pb^{-1} of data written to tape. This is currently being analyzed and new results are expected in the summer of 1993.

References

[1] S.Abachi et al, Submitted to Nuclear Instruments and Methods. See references therein. This is a long paper on the D0 detector

[2] R. Madaras, "Highlights from DØ " Proceedings of the Fermilab meeting of the Division of Particles and Fields of the American Physical Society, C. Albright, P.Kasper, R.,Raja, J.Yoh, editors, World Scientific. See also references herein.

[3] C. Gerber, "W and Z decays into muons at DØ ", Talk given to the American Physical Society, April 1993. DØ Note 1720, Unpublished.

[4] M. Narain,in Proceedings of the 7th APS Division of particles and Fields, Fermilab Nov 10-14 1992. For details, see R.Raja, D0 Notes 1006,1739 (Unpublished).

[5] Q. Zhu, "Status Report on the measurement of the W/Z mass ratio" Talk given to the American Physical Society, April 1993. DØ note 1697 Unpublished.

[6] S.L. Glashow, Nucl. Phys. **22** (1968) 579;
S. Weinberg, Phys. Rev. Lett. **19** (1967) 1264;
A. Salam , in *Elementary Particle Theory*, edited by N.Svartholm (Almquist and Wiksell, Sweden, 1968), p.367.

[7] S.L. Glashow, J. Illiopoulos and L. Maiani, Phys. Rev. **D2** (1970) 1285;
M. Kobayashi and M. Maskawa, Prog. Theor. Phys. **49** (1973) 652.

[8] H. Albrecht et al., Phys. Lett. **B192** (1987) 245;
M. Artuso et al., Phys. Rev. Lett. **62** (1989) 2233;
G. Altarelli and P.Franzini, Z. Phys. **C37** (1988) 271;
J. Ellis et al; Nucl. Phys. **B304** (1988) 205.

[9] F. Abe et al., Phys. Rev. Lett. **64** (1990) 147;
F. Abe et al., Phys. Rev. Lett. **64** (1990) 142; Phys. Rev. **D43** (1991) 664.

[10] UA2 collaboration, T. Åkesson et al; Z. Phys. **C46** (1990) 179;
UA1 collaboration C. Albajar et al., Z. Phys. **C48** (1990) 1.

[11] F. Abe et. al., Phys. Rev. Lett. **68** (1992) 447.

[12] V. Innocenti, Tau polarization and EW parameters at LEP, presented at Rencontres de Moriond, March 14-20, 1993.

[13] P. Nason, S. Dawson and R.K. Ellis, Nucl. Phys. **B303** (1988) 607.

[14] G. Altarelli et al., Nucl. Phys. **B308** (1988) 724;
R.K.Ellis, Fermilab Pub 81/30-T.

[15] F.A. Berends et al., Fermilab Pub 92/196-T. We have used the $t\bar{t}$ cross sections quoted here in E. Laenen, J. Smith, W. van Neerven, Nucl. Phys. **A369** (1992) 543.

[16] F. Paige and S. Protopopescu, BNL Report no. BNL38034, 1986 (Unpublished). We have used the release v6.49 .

[17] User's Guide to GEANT 3.10, R.Brun et al, CERN DD-EE-84-1.

[18] R.H. Dalitz et. al. Phys. Rev. **D45** (1992) 1531.

[19] A. Milder, Dijet Angular Distributions in DØ . Talk given to the American Physical Society, April 1993. DØ Note 1698, Unpublished

[20] V.D. Elvira, Inclusive jet cross sections in DØ . Talk given to the American Physical Society, April 1993. DØ Note 1719, Unpublished.

[21] E. James, B physics using dimuons in DØ . Talk given to the American Physical Society, April 1993.

[22] C. Murphy J/ψ production in DØ . Talk given to the American Physical Society, April 1993. DØ Note 1703, Unpublished.

[23] T. Huehn, A study of $p\bar{p} \rightarrow \mu + X$ at $\sqrt{s} = 1.8$ TeV in DØ . Talk given to the American Physical Society, April 1993. DØ Note 1704, Unpublished.

[24] D. Norman, Leptoquark search in DØ . Talk given to the American Physical Society, April 1993. DØ Note 1702, Unpublished.

Discussion

M.V. Purohit : What is the present limit on m_t from DØ (just to get an idea of detector performance)?

R. Raja : We are not ready to quote a limit yet. At the DPF, with 1 pb^{-1} of data, we see no evidence for an 80 GeV/c^2 top.

X. Tata : You said the machine was delivering 1.5 pb^{-1} per week and DØ was writing 0.8 pb^{-1} per week on tape. Where is the remaining 0.7 pb^{-1} per week going? Also is this expected to improve?

R. Raja : Our main problem is a 20% dead time due to the main ring. Injection and transition in the main ring have to be blanked out. Add to this, stoppages due to high voltage trips, downloading parameters, changing runs make up the rest. Improvements are expected in the letter soon as DØ gets its act together. Main ring problems will be alleviated somewhat when the Tevatron beam lifetime goes of (Stochestic Cooling of the Tevatron is planned). Increased beam lifetime will permit the main ring to be shut down for longer periods during the run.

Probir Roy : Will you be able to study CP-violation in B-physics without the main injector?

R. Raja : I think we will need 1000 pb^{-1} and a good silicon system. We would also like a central field. These three conditions will be met only with Run III and the main injector ($\sim$ 1997).

Probir Roy : What steps are your taking to improve your muon detection?

R. Raja : The muon detection system underwent a loger engineering run in DØ. Since the DPF meeting, the muon system has been aligned, the triggering is being improved, reconstruction code has been improved.

D.P.Roy : Could you comment on the top candidate events in the DØ and the new CDF data?

R.Raja : DØ is presently analysing a candidate $e\mu$ event. Until we understand it better, we prefer to remain silent on it. Expect DØ to say something in 3-4 months.

D.P.Roy : Could you give a realistic schedule of the accumulated luminosity?

R.Raja :

	Begin	End	Projected Luminosity
Run 1a	August 92	May 93	25 pb^{-1}
Run 1b	October 93	October 94	75 pb^{-1} (?)
Run 2 (44 bunches)	$\sim$ October 95		200-300 pb^{-1}

R.M.Godbole : Is your direct γ rate consistent with CDF data?

R.Raja : I belive, within the quoted error bars, the CDF and DØ data are consistent.

A.K.Ray : What is the projected date for looking into CP violation effects in the B-sector with the DØ upgrade set up in Fermilab?

R.Raja : It clearly needs at least a step 1 upgrade of DØ. This implies run 2 which I believe is currently projected at 1995-96. With the solenoid + preshower by 1997-98, we will be in good shape to acquire 1000 pb^{-1} of data. Main injector will also come into being in that time frame.